THE JOURNAL OF PHYSICAL CHEMISTRY C

Article

pubs.acs.org/JPCC

Heterogeneity in Dye–TiO_2 Interactions Dictate Charge Transfer Efficiencies for Diketopyrrolopyrrole-Based Polymer Sensitized Solar Cells

Ajay Jha,[†] Vineeth B. Yasarapudi,[†] Hadiya Jasbeer,[†] Catherine Kanimozhi,[‡] Satish Patil,[‡] and Jyotishman Dasgupta*[,†]

[†]Department of Chemical Sciences, Tata Institute of Fundamental Research, Mumbai 400005, India

[‡]Solid State and Structural Chemistry Unit, Indian Institute of Science, Bangalore 560012, India

Supporting Information

ABSTRACT: Power conversion efficiency of a solar cell is a complex parameter which usually hides the molecular details of the charge generation process. For rationally tailoring the overall device efficiency of the dye-sensitized solar cell, detailed molecular understanding of photoinduced reactions at the dye-TiO_2 interface has to be achieved. Recently, near-IR absorbing diketopyrrolopyrrole-based (DPP) low bandgap polymeric dyes with enhanced photostabilities have been used for TiO_2 sensitization with moderate efficiencies. To improve the reported device performances, a critical analysis of the polymer–TiO_2 interaction and electron transfer dynamics is imperative. Employing a combination of time-resolved optical measurements complemented by low temperature EPR and steady-state Raman spectroscopy on polymer–TiO_2 conjugates, we provide direct evidence for photoinduced electron injection from the TDPP-BBT polymer singlet state into TiO_2 through the C═O group of the DPP-core. A detailed excited state description of the electron transfer process in films reveals instrument response function (IRF) limited (<110 fs) charge injection from a minor polymer fraction followed by a picosecond recombination. The major fraction of photoexcited polymers, however, does not show injection indicating pronounced ground state heterogeneity induced due to nonspecific polymer–TiO_2 interactions. Our work therefore underscores the importance of gathering molecular-level insight into the competitive pathways of ultrafast charge generation along with probing the chemical heterogeneity at the nanoscale within the polymer–TiO_2 films for optimizing photovoltaic device efficiencies.

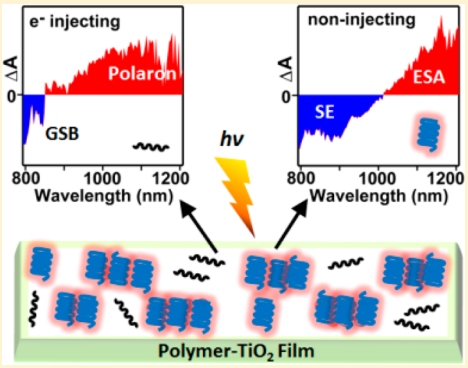

1. INTRODUCTION

The quest for clean, cheap, and sustainable energy has led to the development of organic solar cells (OSCs) in the past two decades.[1−6] OSCs offer great design flexibility due to the enormous possibilities of rationally tailoring the principal molecular components iteratively based on their observed optoelectronic properties. Additionally, the device costs can drastically be reduced by developing new solution processable techniques for large-scale fabrication of organic electronics.[7,8] These advantages compel researchers to develop new materials and explore novel device architectures for fabricating economically viable organic solar cells.[9−11] The dye-sensitized solar cells, conceptualized through the pioneering work done by Michael Graetzel,[12] have been a cheap alternative, using an efficient dye to trap light and carry out charge separation chemistry across an organic–TiO_2 interface. All-organic dye based DSSCs have reached 8–9% efficiency[13] although their photocycling stabilities have been questionable.[14] Usually small molecule dyes have very limited absorption range due to the spatially localized electronic transitions. However, constructing extended structures by linking donor–acceptor (D-A) moieties via π-linkers have helped in pushing the absorption window toward the near-IR part of the electromagnetic spectrum.[15,16] Alternatively, one can synthesize conjugated polymers from smaller D–A monomers,[17,18] and thereby broaden the absorption profile as well as increase the absorption cross-section.[19] These classes of low bandgap polymers show lower exciton binding energies than homopolymers like P3HT and PPVs which ensures reduced thermodynamic penalty for charge separation at the interfaces.[11,20] Additionally they usually have low HOMO energies which lead to an increase in the open circuit voltage (V_{OC}) as well as better stability for the active material. The discernible advantage provided by the viscous nature of these polymer solutions ensures a facile film formation process on the TiO_2 surface thereby making device fabrication reproducible.[21]

Diketopyrrolopyrrole-based (DPP) conjugated polymers have recently shown tremendous promise for fabricating a

Received: October 26, 2014
Revised: November 19, 2014
Published: November 19, 2014

   dx.doi.org/10.1021/jp510733k | J. Phys. Chem. C 2014, 118, 29650–29662

new generation of BHJ solar cells, organic light emitting diodes (OLEDs), and organic thin film transistors (OTFTs).[22−26] The exciting properties of these materials emanate from their admirable charge carrier mobility[25,27] and exceptional photo/thermal-stability.[22,28] DPP-based molecular units have been used as π-linkers in D−A based organic dyes for Graetzel-type cells.[13,29,30] The absorption window in such dyes have been limited to 550 nm which is constrained by the length of the DPP linker.[31] Recently, Sharma et al. reported commendable (~2%) power conversion efficiencies of DSSCs using a red-absorbing (>650 nm) conjugated D−A polymer comprising of 9−10 repeat units of thiophene diketopyrrolopyrrole−4,8-dihexylloxybenzo[1,2-b;3,4-b]dithiophene (TDPP-BBT).[32] The measurement of solar cell power conversion efficiencies does not capture the molecular basis for charge generation[33] and transport in such devices.[34] Using a combination of femtosecond transient absorption spectroscopy, low-temperature electron paramagnetic resonance and steady state resonance Raman measurements, we provide direct evidence for an impaired charge transfer efficiency in polymer−TiO_2 films due to fast charge recombination rate combined with pronounced ground state heterogeneity in polymer−TiO_2 films. Nonspecific polymer−TiO_2 interactions lead to a dominant fraction of noninjecting polymer population. Only a minor chemically competent population does charge injection to TiO_2 within <110 fs via the C═O group of the DPP unit although with a picosecond recombination time scale.

2. EXPERIMENTAL DETAILS

Steady State Absorption and Emission Measurements. Absorption measurements in solution were carried out in SPECORD 205 spectrophotometer. SPEX Fluorolog model 1681T (T-format) spectrofluorimeter was used to carry out steady-state fluorescence measurements of TDPP-BBT in different solvents. The emission quenching experiment for free and bound TDPP-BBT in solution was carried out at the same polymer concentration. Diffuse reflectance measurements of polymer−TiO_2 were carried out in JASCO V-530 rendered with a diffuse reflectance auxiliary.

Surface Coverage of Polymer over TiO_2 (P25). Surface coverage of the polymer was estimated by measuring the optical density of the free polymer after repeated washing of the bound fraction subsequent to preincubation of the polymer with TiO_2 nanoparticles.[35] To estimate the coverage, a solution of TDPP-BBT was prepared by adding 1.0 mg in 5 mL of chloroform. Absorption spectrum of stock solution [Figure S4 in Supporting Information; (in black)] was collected to ascertain the concentration of the polymer before loading. 1.0 mg of TiO_2 was suspended in 1.5 mL of TDPP-BBT solution and homogenized for 4 h. For control experiment, 1.0 mg of TiO_2 was suspended in 1.5 mL of chloroform and homogenized. These solutions were centrifuged at 13,000 rpm for 10 min at room temperature and the supernatant were collected subsequently. Absorption spectrum of the polymer in the supernatant solution (Figure S4 in red) was monitored to determine the concentration of free polymer relative to the control sample. The pellets of TiO_2−polymer were resuspended in 1.5 mL of chloroform and homogenized for 2 h and then centrifuged. The above-mentioned procedure for concentration determination was repeated 2−3 times until the supernatant solution (Figure S4 in blue) showed no measurable absorbance. Amount of the polymer bound to TiO_2 was calculated from the differential change in the absorbance with respect to the stock solution. We estimated that ~10% of the polymer has been bound to TiO_2 surface sites at a given concentration of TiO_2. To know coverage of the polymer over TiO_2 nanoparticle, we calculated concentration of surface Ti sites.[36] The molar concentration of surface Ti sites, $[Ti_{surf}]$ is given by

$$[Ti_{surf}] = \frac{[TiO_2]*12.5}{D}$$

where $[TiO_2]$ is the molar concentration of TiO_2 and D is the diameter of the particle which was 25 nm for our TiO_2 sample. Coverage of the polymer over TiO_2 was calculated by taking ratio of amount of bound polymer with $[Ti_{surf}]$. We therefore deduce that only ~1 molecule of TDPP-BBT is available for 1000 $[Ti_{surf}]$ sites.

Photoinduced EPR Measurements. Photoinduced EPR spectra of both the pure TiO_2 and polymer−TiO_2 mixture were recorded in a TE011 cavity on a Bruker EMX Micro X-band spectrometer. Since no signals were observed at room temperature, the measurements were performed at low temperature with operating frequency at 9.31388 GHz. For all the measurements the samples were degassed to remove oxygen and the temperature was set to 80 K using a home-built temperature cooling and sensing unit. For recording the EPR spectra, MW power of 0.2 mW was found to be optimal with modulation amplitude of 1 G at 100 kHz modulation frequency. The illumination in the visible range was done using a xenon lamp with a UV filter while the power was kept at ~10 W focused on to the frozen sample through a transparent window of 5 mm size. Both dark and illuminated spectra were recorded separately, and light-minus-dark spectra were interpreted for trapped spins in either the polymer or the TiO_2 nanoparticle. Post illumination the sample was remeasured in the dark to check for reversibility at 80 K.

Polymer−TiO_2 Film Preparation. For film fabrication, a square UV-transparent quartz substrate of 2.5 cm was cleaned in hot piranha solution which was made from a mixture of 96% H_2SO_4 and 30% H_2O_2 in a 2:1 v/v ratio and then rinsed with deionized water. The cleaned quartz substrate was then dried in an oven at 120 °C for few hours and was subsequently treated under UV light for 2 h before casting the polymer film. For making the titania paste, TiO_2 powder (1 mg) was dissolved in 2 mL of chloroform and was ground in a porcelain mortar in order to break the aggregates into separate particles. The thick paste was coated on the cleaned quartz substrate and dried in air. The air-dried film was kept in oven at 150 °C for 1 h. This TiO_2 coated plate was dipped in a polymer solution comprised of 1 mg of TDPP-BBT dissolved in 2 mL of chloroform, in a Petri-plate for 4 h. During this period, the Petri-plate was covered with aluminum foil and kept in dark to avoid light. Polymer bound TiO_2 plate was taken from this solution and washed with excess of chloroform to remove physisorbed polymer molecules. This polymer−TiO_2 film was sealed by scratching off the film on the edges of the substrate, applying adhesive and then finally covering with another cleaned quartz plate in argon atmosphere. The steady state absorption of this film was recorded using a diffuse reflectance spectrometer. The prepared polymer−TiO_2 film was used for Raman and time-resolved absorption measurements. For Raman measurements on the neat polymer film, fabrication of the polymer film was done following the reported procedure by Banerji et al.[37] Briefly, a square quartz substrate (2.5 cm, thickness = 2 mm) was used and cleaned using the same protocol mentioned in

dx.doi.org/10.1021/jp510733k | J. Phys. Chem. C 2014, 118, 29650−29662

polymer−TiO_2 film preparation. The polymer solution for the film was prepared by dissolving 4 mg/mL chlorobenzene which was stirred overnight at 50 °C. This solution was drop-casted on the cleaned quartz substrate and then annealed on a hot plate at 60 °C for 1 h under nitrogen atmosphere. This film was then cooled to room temperature and kept for few hours in nitrogen atmosphere before it was sealed using another cleaned square quartz substrate using epoxy resin at the edges.

Time-Resolved Absorption Measurements. All pump−probe measurements have been carried out using a transient absorption spectrometer as described before.[38] Briefly, the output of a 400 mW Ti:sapphire laser-based oscillator with bandwidth of ∼90−100 nm and 80 MHz repetition rate (Coherent Micra-5 Modelocked Titanium: Sapphire Laser system) was amplified using pulse chirped amplification using a Coherent Legend Elite amplifier laser system. The ∼4 mJ/30 fs output from the amplifier at 1 kHz repetition rate is split by a 50:50 beam splitter to generate the excitation pump pulse and the low power probe pulse. The 650 nm pump pulse is generated using an optical parametric amplifier (Coherent OPeraASolo Optical Parametric Amplifier system) and attenuated to ∼100−200 nJ by a neutral density filter for solution measurements. The path length of the pump beam is actively controlled by a computer through a quadra-pass mirror assembly (Newport) to vary the time delay between pump and probe pulses. White light probe is generated by focusing a portion of the fundamental 800 nm on a 2 mm thick sapphire crystal, while the generated visible and NIR regimes of the probe continuum are separated using a 750 nm filter. The intensity of the 800 nm beam is attenuated by iris and neutral density filter to achieve a stable probe from 400 to 1400 nm. This probe, after passing through the sample, is dispersed onto an imaging element (297 pixels) after entering through a Helios spectrograph. Polarization of the pump pulse is kept at magic angle (54.7°) for all the measurements to remove any effect of rotational diffusion. The wavelength sensitive instrument response function (IRF) was measured using optical Kerr-effect (OKE) arrangement on a 1 mm thick glass with $\lambda/4$ polarizer (in pump path) and an analyzer (in the probe path). The IRF for 650 nm excitation pump and visible probe was found to be ∼90 fs which was later used in the kinetic fitting procedure.

For all time-resolved measurements, the free polymer solution was made by weighing out 1 mg of the polymer TDPP-BBT in 5 mL of chloroform. The transient absorption measurements in solution state were carried out in a flow cuvette with 0.5 mm path-length with the liquid driven by a peristaltic pump. The flow rate was maintained in order to refurnish a fresh sample before every shot. For all TiO_2 samples, 1 mg of polymer was added to 5 mL of a $CHCl_3$ solution containing 1 mg dry weight of TiO_2. The polymer−TiO_2 sample was transferred into a 2 mm thick cuvette with a magnetic stir bar used to constantly replenish the sample for each data point. Transient absorption spectra are obtained after averaging 1500 shots for each time delay between pump and probe pulses. The sample integrity was checked using absorption measurements before and after each pump−probe experiment.

Pump−probe measurements on films were recorded to probe the near-infrared region after excitation at 650 nm with 12 μJ cm^{-2} pulses with >300 μm beam size at the focus. These measurements were carried out in the linear excitation regime to avoid bimolecular decay processes which was checked by carrying out pump power dependence at different pump fluence. Transient absorption spectra are obtained after averaging 500 shots at each time delay between pump and probe pulses. To check the stability of the film after the experiment, same experiment was again repeated on the same focal spot which showed no change in the kinetics (Supporting Information, Figure S11). Measurements were also performed on different spots on the film which showed similar kinetics. For film measurements, IRF for 650 nm excitation pump and NIR probe was found to be ∼110 fs.

An extended analysis of these transient spectra has been performed. The data treatment involves time correction to account for the chirp of the probe pulse. The kinetic analyses were carried out using IGOR pro 5 with programs written to deconvolve the time-constants from the measured IRF (for details see the Supporting Information). Pump−probe spectra obtained for the free and bound polymer were subjected to global analysis to obtain decay associated spectra. The principal components were evaluated using commercial Surface Xplorer software.

Fluorescence Upconversion Measurements. For all time-resolved emission measurements we followed the same procedure for sample preparation as already described for the transient absorption measurements. The fluorescence upconversion measurements were carried out on FOG 100 as described previously.[39] The excitation beam at 420 nm was generated by doubling the fundamental output from a mode-locked Ti:sapphire laser (Tsunami, Spectra Physics) femtosecond oscillator operating at 100 MHz. To minimize photobleaching, power of the excitation pulse was attenuated to ∼5 mW, and the samples were placed in a rotating cell to replenish the sample for each data point. The fluorescence from the sample was upconverted in a nonlinear crystal by mixing it with the gate pulse, which is derived from the laser fundamental. The gate beam was directed toward the crystal via a computer-controlled delay stage to get the time profile of this upconverted signal. This upconverted light is detected using photon counting electronics after being dispersed by a monochromator. The fluorescence decays were recorded at magic angle polarization with respect to the excitation pulse. IRF of 340 fs was obtained with cross-correlation experiment using the Raman scattering from ethanol. The kinetic decays were fitted by convoluting the multiexponential decay functions with the measured IRF.

Resonance Raman Measurements. Resonance Raman measurements were performed on the Alpha 300R confocal Raman microscope, WITec GmbH, Ulm (Germany), using 532 nm excitation source which was taken from a solid-state frequency doubled DPSS Nd:YAG laser (WITec). A 20× objective was used to focus the beam into the solution flowing through a capillary with 1 mm diameter. The back scattered light was put into a lens-based ultrahigh throughput spectrometer (UHTS300) using a 100 μm optical fiber. A back illuminated CCD-camera (1024 × 128 pixels, Peltier-cooled to −65 °C) is coupled to the spectrograph with 1800 grooves/mm grating for detection. The spectral resolution of the spectrograph was ∼2 cm^{-1}. To prevent photodamage, all the solution measurements were done in the flowing conditions using a homemade flow-system. The power of the incident excitation beam at the sample was attenuated to ∼3 and ∼0.5 mW for solution and film measurements, respectively. Spectra were recorded with an integration time of 30 and 5 s for solution and film measurements, respectively. For all RR

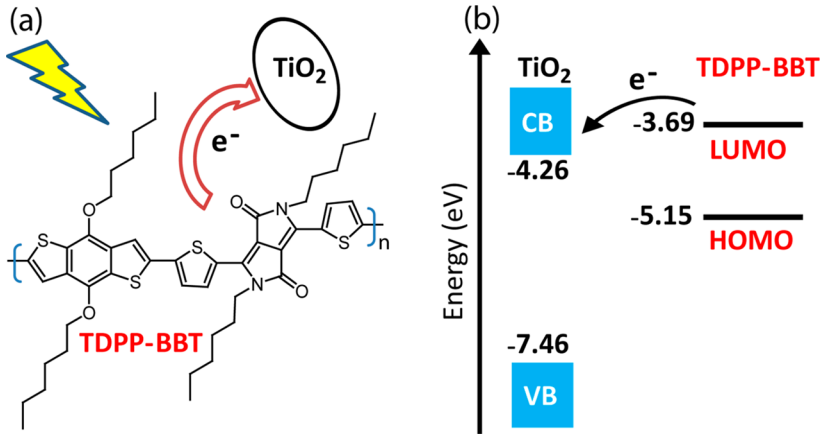

Figure 1. (a) Chemical structure of the polymer thiophene diketopyrrolopyrrole−4,8-dihexylloxybenzo[1,2-b;3,4-b]dithiophene (TDPP- BBT); (b) energy band diagram of TDPP-BBT:TiO_2 representing energetically favorable electron transfer reaction from LUMO of the polymer to conduction band of TiO_2.

spectra, the TiO_2 Raman scattering features along with neat solvent spectra were subtracted. All the peaks were assigned based on the DFT calculations carried out at the B3LYP/6-311g(d,p) level in the gas phase.

3. RESULTS AND DISCUSSION

TDPP-BBT polymers have been used as photoactive materials for dye-sensitized solar cells due to their good near-IR absorption cross sections and photostability of the DPP unit. Figure 1a describes the chemical backbone of the polymer's monomer unit, and the conjectured photoinduced electron transfer process relevant to the DSSC operation. The energy ordering of the HOMO and LUMO levels for this low-band gap polymer is shown in Figure 1b.[40] The electron injection from the LUMO is thermodynamically favorable by 570 meV. In the next few sections, we describe the fundamental characterization of this favorable electron transfer dynamics by precisely probing the polymer−TiO_2 interactions and excited state evolution both in solution and in solvent casted films.

Steady-State Absorption and Emission Measurements of TDPP-BBT in Solution. The TDPP-BBT monomeric unit consists of a DPP core with 8π electrons in two fused lactam rings having alkylation on lactam N atoms to improve its solubility in common organic solvents like chloroform and dichloromethane as shown in Figure 1a. The DPP-based monomer unit is synthesized by covalently linking it to a BBT unit which provides the donor functionality via a hole conducting thiophene linker.[32] The specific derivitization of the TDPP-BBT unit was chosen primarily to tune the band gap toward ∼1.4 eV in this D−A pair. The absorption spectra of TDPP-BBT free in solution and bound to TiO_2 in chloroform is shown in Figure S1. The TDPP-BBT solution exhibits a band in the UV at 370 nm and a broad absorption with a band maximum at 655 nm which primarily arises from a strongly allowed dipolar excitation on the TDPP core along with a contribution from an intramolecular charge transfer (CT) excitation on the TDPP-BBT unit.[32] To confirm the partial contribution of the intramolecular CT transition, we measured the absorption maxima of the visible band in solvents with different polarity including chloroform, chlorobenzene, dichloromethane, and tetrahydrofuran. Figure 2a shows a ∼12 nm red-shift for the polymer absorption maxima in nonpolar

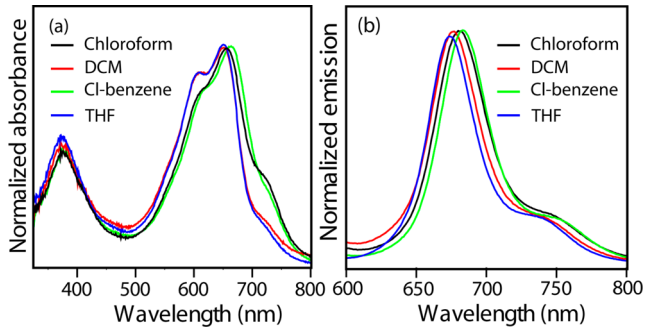

Figure 2. (a) Steady state absorption of the TDPP-BBT in different solvents: chloroform (black), dichloromethane, DCM (red), chlorobenzene (green), and tetrahydrofuran, THF (blue); (b) steady state fluorescence spectra of the TDPP-BBT in chloroform (black), dichloromethane, DCM (red), chlorobenzene (green), and tetrahydrofuran, THF (blue) after 590 nm excitation.

solvents in comparison to polar solvents possibly due to ground state destabilization of the dipolar backbone. Alternatively this shift could be explained by conformational heterogeneity of the polymer in different solvents as evident from the altered intensity in the vibronic feature ∼725 nm.

Similarly, steady state emission spectra of TDPP-BBT obtained subsequent to excitation at 590 nm in various solvents clearly shows moderate polarity dependence (Figure 2b). Emission spectrum of the TDPP-BBT polymer in solution is narrow as compared to that of absorption indicating emission possibly emanates from the a specific set of chromophores; that is, the most conjugated conformational unit or the excited state has more homogeneous population as compared to the ground state.[41] Additionally, we observe a modest Stokes shift of ∼620 cm^{-1} in the polymer which closely mirrors the Stokes shift of the TDPP core unit in solution (Figure S2). The blue shift of the emission maxima in highly polar solvents like dichloromethane suggests ground state stabilization of the dipolar D−A backbone plays an important role along with weaker interchain coupling in such solvents.[42] To ascertain whether the stabilization is across the entire TDPP-BBT unit, we benchmarked the solvent dependence of the TDPP-centric dipolar excitation using just the parent TDPP monomer unit as shown in Figure S2. The moderate polarity dependence observed based on the linear correlation in the Stokes shift vs

dx.doi.org/10.1021/jp510733k | J. Phys. Chem. C 2014, 118, 29650−29662

polarity index for the TDPP core highlights the strongly allowed dipolar transition (see Figure S17 in the Supporting Information). For the TDPP-BBT polymer no such linear correlation was observed indicating that the role of solvent dependent polymer conformational heterogeneity is significant which makes it difficult to explicitly assign this change to partial ICT contribution in the donor−acceptor backbone. However, the red-shift in the electronic resonance of the TDPP-BBT polymer compared to the TDPP core absorption can be explained by a delocalized HOMO and a TDPP-localized LUMO (Figure S3 in the Supporting Information) as gathered by density functional theory (DFT) calculations at the B3LYP/6-31G** level on the geometry optimized TDPP-BBT methyl-substituted monomer.

Steady-State Absorption and Emission Measurements of Polymer−TiO_2 in Solution. A significant part of the power conversion efficiency of any dye-sensitized solar cell is dictated by the fundamental dye−TiO_2 interaction. In order to completely understand this interaction, TiO_2 nanoparticles were added to the solution of free polymer. The absorption band maxima is not significantly affected but the profile broadens slightly due to increased heterogeneity in the sample induced by chemical interaction with the nanoparticle as shown previously by Patil and co-workers (Supporting Information, Figure S1).[32] This broadening on the red side of the transition helps in enhancing light harvesting beyond 800 nm. Additionally, due to pronounced scattering of the polymer−TiO_2 solution and presence of overlapping TiO_2 band edge, the absorption profile of the polymer shows a broad baseline that continuously rises rendering the second absorption feature invisible. The scattering primarily arises due to the presence of the 25 nm TiO_2 nanoparticles. The lack of a prominent spectral change in the absorption profile implicates possibly a weak interaction with the TiO_2. A surface coverage experiment which is described in the Experimental Section suggests that only ∼10% of the polymer is bound to TiO_2 while rest is free in solution. Therefore, critical analysis of the described steady state and time-resolved spectroscopic data in solution has to be inclusive of a model which takes into account the 10% bound fraction of the polymer. Steady state emission spectrum of the polymer in the presence of TiO_2 in chloroform shows a quenched emission at 675 nm compared to the free polymer (Figure 3a). Absorption normalization of the polymer feature was done for removing any scattering artifacts. Assuming 90% fraction of free polymer in solution, the quenching possibly arises from pronounced lifetime quenching of the bound fraction. Energy transfer quenching can be ruled out based on the low spectral overlap of the polymer's visible absorption feature and the band gap of TiO_2 particles. We assigned this quenching pathway to the electron injection from the photoexcited singlet state of the polymer to TiO_2, the chemistry which makes this polymer a potent photovoltaic material.[32]

Low-Temperature EPR Measurements. The potency of the TDPP-BBT polymer for photoinduced electron injection in TiO_2 was determined by probing the spectral signatures of the trapped spins in both polymer and TiO_2. Electron paramagnetic resonance (EPR) experiments were used to detect the radical cation generated on the polymer backbone. At room temperature and under illumination no steady state EPR signal was observable possibly due to the fast injection and recombination associated with the charge generation process. However, upon lowering the temperature to 80 K and ensuring good insulation

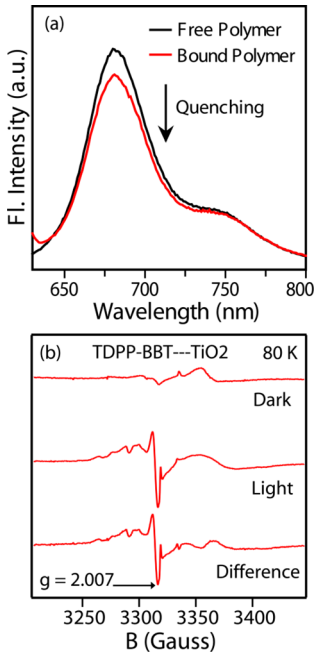

Figure 3. (a) Steady state fluorescence of the free polymer TDPP-BBT (black) and the TiO_2 added solution of the polymer (red) in chloroform when excited at 600 nm indicating fluorescence quenching in the presence of TiO_2. In both the samples, the concentration of the polymer was kept the same; (b) photoinduced EPR spectra of TDPP-BBT on TiO_2 during excitation with visible light source while samples were kept at 80 K. The difference spectrum represents light induced spectral changes obtained after correction for dark signals. The cation radical of the polymer is observed at g = 2.007.

from O_2 gas, photoinduced EPR signals were observed. Figure 3b shows the photogenerated EPR signals after a careful subtraction from the dark spectral signatures. The light-minus-dark difference EPR spectrum of TiO_2 bound TDPP-BBT shows distinct radical peak at g = 2.007 which is assigned to TDPP-BBT cation radical species or the polaron. The EPR signal from electron trapped in TiO_2 conduction band is too broad to be observed.[43] The dark EPR spectrum represents background signal arising from defects in commercial TiO_2 particles which was confirmed by independent measurements. To ensure the validity of our radical cation assignment, photoinduced EPR spectrum of pure TiO_2 at 80 K was recorded as a control and is shown in Figure S5 in the Supporting Information. The difference spectrum in TiO_2 only sample shows a broad signal at g = 1.93 which have been previously ascribed to photogenerated Ti^{3+} centers in amorphous TiO_2.[44] Signal with g values of 2.02, 2.01, and 2.00 have been reported to those corresponding to Ti^{4+}−O^{2-} species. The EPR signal for the polaronic feature in the polymer therefore represents compelling evidence that TiO_2 associated TDPP-BBT polymer can inject electrons although it does not provide sufficient evidence to discriminate between the singlet or triplet state injection mechanism. Dynamic spectroscopy was carried out to determine the electron transfer mechanism from the relevant polymer electronic state.

Transient Absorption Measurements in Solution. To gather a mechanistic understanding of the excited state dynamics and the kinetics of electron injection, we carried out transient pump−probe spectroscopy on the pure polymer and its TiO_2 conjugate both in solutions and films. Conjugated polymers usually have complex excited state dynamics after the

dx.doi.org/10.1021/jp510733k | J. Phys. Chem. C 2014, 118, 29650−29662

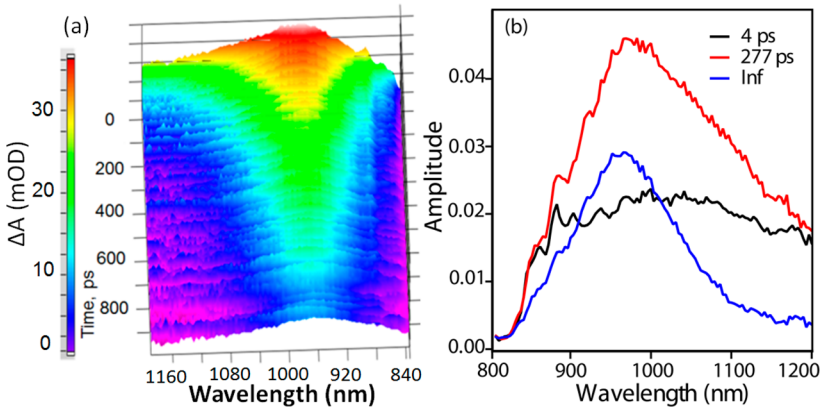

Figure 4. (a) Three-dimensional representative plot of the excited state absorption (ESA) profile for NIR probe wavelengths after subjecting the free polymer in chloroform to photoexcitation at 650 nm. The intensity color code is shown on the left. (b) Principal spectra of three states S_1^{hot} (black line), S_1^{cold} (red line), and T (blue line) obtained after singular value decomposition (SVD) of pump−probe data in the NIR region of the free polymer.

creation of the singlet exciton. Subsequent to photoexcitation at 650 nm, we monitored the transient electronic changes in the near-IR (NIR) window from 800 to 1200 nm with a temporal precision of ∼90 fs. An intense excited state absorption (ESA) feature at 969 nm representing the singlet exciton feature was observed immediately after photoexcitation, shown in Figure 4a. The ESA feature narrowed within 5−10 ps thereby indicating relaxation in the excited band of states. Such relaxation pathways have been reported previously for PPV and P3HT class of conjugated polymers thereby implying a direct evidence for localization of excitonic feature on few polymer chains after the delocalized photoexcitation.[45,46] The ESA profile between 800 and 1100 nm was resolved into its principal components based on the significance value of each of the components.[47] The singular value decomposition (SVD) revealed three components in the spectra (Figure 4b) with lifetimes of 4 ps, 277 ps and a nondecaying component assigned here to be the triplet state (T) based on global fit to the data by a target model shown in Figure 5a. The 4 ps component appears to be very broad ranging from 800 to 1100 nm with a peak at ∼1050 nm denoting the delocalized exciton. The 277 ps component representing the localized singlet exciton is centered at 980 nm and appears much narrower with more intense transition possibly due to localization via conformational relaxation through torsional modes.[48−50] We therefore assign the 4 ps component to a delocalized singlet state (S_1^{deloc}) while the long-lived component as the conformationally relaxed localized singlet state or S_1^{loc}. The assignment of the 277 ps component to a relaxed singlet population was supported by lifetime measurements through time-correlated single photon counting (TCSPC) measurements which also yielded long lifetime for the singlet exciton as shown in Figure S6 (Supporting Information). The free polymer showed a mean lifetime of ∼450 ps indicating emission from the long-lived relaxed singlet exciton state. The fate of the relaxed singlet state is determined by pathways which include intersystem crossing (ISC) to the nondecaying triplet (T) state as well as the electronic relaxation back to the ground state of the polymer. The assignment of the triplet state was based on previous studies carried out by Janssen and co-workers who had shown that the triplet absorption of the TDPP backbone usually occurs between 860 and 1000 nm depending on the extent of conjugation.[51] They show examples of two TDPP molecules with a different number of thiophenes attached. Although our feature is at ∼960 nm, it is spectrally broader (fwhm ∼1350 cm^{-1}) than what was reported by Janssen et al. for the TDPP monomer (fwhm ∼450 cm^{-1}) possibly due to the extent of polymer heterogeneity in solution. However, the T feature is much narrower than the singlet exciton delocalized or the localized ESA feature.[52]

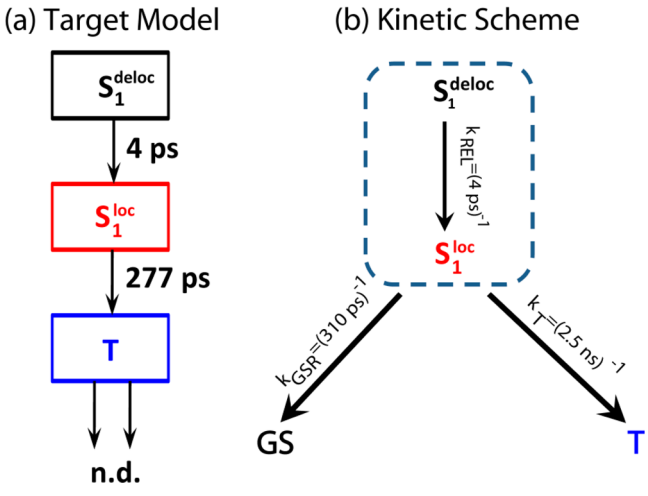

Figure 5. (a) Sequential target model was used to fit the pump−probe data for TDPP-BBT in chloroform, and the lifetimes obtained are shown. (b) Kinetic scheme with analyzed rate constants based on ground state recovery (GSR) dynamics and excited state absorption kinetics in NIR.

The lifetime of the relaxed singlet state is dictated by the ground state recovery (GSR) dynamics and triplet state formation. To determine the intrinsic kinetic rates for interconversion between individual states, population decay kinetics was obtained at wavelengths where the triplet contribution is negligible. In order to capture the ground state recovery dynamics, transient visible data after excitation at 670 nm were collected for the free polymer shown in Figure S7. The GSR was measured at 612 nm which is slightly bluer to the excitation wavelength within the ground state bleach signal after photoexcitation at 670 nm using visible femtosecond pump−probe spectroscopy, shown in Figure S8. The exponential fit to the data indicated the presence of a 310 ± 80 ps time

dx.doi.org/10.1021/jp510733k | J. Phys. Chem. C 2014, 118, 29650−29662

component along with a small nondecaying part arising from nonrecovery of the ground state within 2.5 ns time-window due to triplet formation (see Table ST1). The ∼310 ps recovery to ground state implies that the triplet should be formed with a time constant of >2.5 ns since the effective lifetime of relaxed singlet state is 277 ps due to kinetic partitioning. The entire kinetic scheme shown in Figure 5b therefore captures the complexity of excited state dynamics of the polymer in solution and also presents the pathways through which the photon energy can be best utilized.

The electron injection dynamics in TiO_2 added polymer solution was probed using the population decay dynamics observed for the ESA feature at 1090 nm since the kinetics will reflect the depopulation pathways of the singlet exciton state. We plotted the singlet exciton decay kinetics at 1090 nm of the TDPP-BBT polymer both in its free form and in TiO_2 solutions as shown in Figure S9 in the Supporting Information. The kinetics is fitted to multiexponent fit in convolution with the IRF of ∼90 fs. The free polymer showed two time-constants τ_1 = 5 ± 0.7 ps and τ_2 = 330 ± 40 ps (see the Supporting Information, ST1). The fast time-component of 5 ps was assigned to the conformational relaxation in the singlet exciton state. The long time-constant of ∼330 ps represents the time scale of the loss of the relaxed singlet state. In the presence of TiO_2, the time-constant $\tau_1 \approx 4.6 \pm 3$ ps appears along with a long component τ_2 = 380 ± 240 ps. Both the time constants for TiO_2 added samples have much larger errors due to the scatter in the data as shown in Figure S9. The short component is rather indistinguishable from the free polymer data as the dynamics is dominated by the free polymer. The lack of precise determination of the injection dynamics indicates low population sensitivity of the transient absorption measurement in solution due to a dominant overlapping contribution from the free form.

Time-Resolved Emission Measurements in Solution. In order to sensitively follow the electron injection rate in colloidal suspension, multiwavelength time-resolved fluorescence kinetics was carried out to quantify the pure singlet exciton lifetime change. We measured the fluorescence decay kinetics in the time-domain using femtosecond fluorescence upconversion technique with an instrument response function (IRF) of ∼340 fs at 650 and 700 nm as shown in Figure 7. The time-resolved emission arising from free polymer (black circles) shows three decay components of τ_1= 2.5 ± 1 ps and τ_2 = 23 ± 6 ps and a long component (>500 ps) after convoluting with the IRF. The ∼2.5 ps component is assigned to the intrachain torsional relaxation analogous to the well characterized pathway operative in conjugated polymer P3HT.[49] The 23 ps decay component, although unassigned, can be conjectured to represent the energy transfer across individual polymer chains. The >500 ps longer component was more reliably measured using time-correlated single photon counting (TCSPC) method. A wavelength dependence of the time-resolved emission process measured via fluorescence upconversion reveals two different emissive states. The fluorescence photons detected at 650 and 680 nm reveal instantaneous or IRF limited rise of primary emission from the immediately excited singlet state as shown in Figure S10 (Supporting Information). However, when the emitted photons at 700 nm are collected in a time-gated manner, a rise time of 2.5 ps emerges which corresponds to the rise of a relaxed exciton emitting at >700 nm as shown in Figure 6 (Table ST2 in the Supporting Information). Exciton dynamics in polymers have been

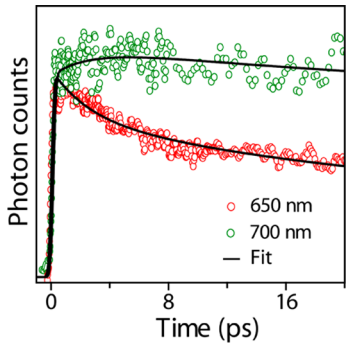

Figure 6. Fluorescence upconverison data of the free polymer in chloroform with λ_{ex} = 410 nm and λ_{em} at both 650 nm (in red circles) and 700 nm (in green circles) along with the best fits to the data. IRF of fluorescence upconversion measurements was ∼340 fs. The rise time observed in the 700 nm data indicates delayed emission due to intrachain relaxation of the singlet exciton.

reported to show a pronounced electronic relaxation effect due to torsional motions across the polymer backbone.[37,49] In addition, the absence of pronounced changes in solvent dependent steady state emission spectra indicates that this relaxation possibly occurs within the excited band of states independent of solvation. Therefore, our wavelength-dependent time-resolved emission measurements of the free TDPP-BBT polymer give insight into the excited state relaxation pathway of the photoinduced singlet state. For productive charge generation without loss of photon energy, the viability of electron injection from the immediately prepared hot singlet state should be faster than the relaxation time scale.

The TiO_2 added polymer sample showed scattering upon excitation and resulted in loss of overall detected photons. Therefore, the experiments were done with an integration time twice that of the free polymer thereby making the photon collection effective. The polymer with TiO_2 in solution shows an extra ultrafast subpicosecond decay component of τ_1= 0.6 ± 0.2 ps other than the three components seen previously in the free polymer namely τ_2 = 3 ± 2 ps and τ_3 = 13 ± 1.5 ps and a long component shown in Figure S11a, Supporting Information. Although the amplitude of the short ∼600 fs exponent was found to be ∼9%, the appearance of this ultrashort decay component becomes obvious when compared to free polymer within the 5 ps time window as shown in the Supporting Information, inset of Figure S11a. The observation of small amplitude for the ultrafast component relates to the poor effective coverage of the polymer on TiO_2. The appearance of an ultrafast subpicosecond component beyond the ∼3 ps relaxation time scale displays the sensitivity of the emission process toward revealing an additional ET channel in the excited state dynamics of the polymer. Additionally, the 13 ps component observed demonstrates the sensitivity of the excited state energy transfer pathway due to the presence of TiO_2 nanoparticles. The temporal shortening of this pathway provides unequivocal evidence for altered polymer−polymer interactions due to inclusion of polymer−TiO_2 interfaces. Since we have already calculated that only 10% of the total polymer represents the bound fraction to TiO_2, the fast decay rate of ∼600 fs is assigned to ET process from this fraction. This rate compares favorably with the rates reported previously for conjugated polymers of the PPV family when bound to TiO_2 in solution.[8] However, the singlet exciton relaxation time scale indicates that the injection takes place from the unrelaxed

dx.doi.org/10.1021/jp510733k | J. Phys. Chem. C 2014, 118, 29650−29662

singlet state, which mechanistically implies an effective photon-energy conserving ET injection. Therefore, based on the data obtained from transient kinetics and fluorescence upconversion measurements, a generalized microscopic kinetic scheme is presented in Figure S11b (Supporting Information). The time scale of the singlet state relaxation (3−4 ps) competes with the subpicosecond ∼0.6 ps electron transfer time scale to TiO_2.

Transient Absorption Measurements in Polymer−TiO_2 Films. In order to gain a direct spectroscopic access on the bound fraction and probe the polymer−TiO_2 interactions, we tracked the transient dynamics in degassed dip-coated polymer−TiO_2 films. Transient pump−probe measurements were performed on a polymer−TiO_2 film using 650 nm pump wavelength and near-infrared probe at 800−1200 nm. Figure 7a

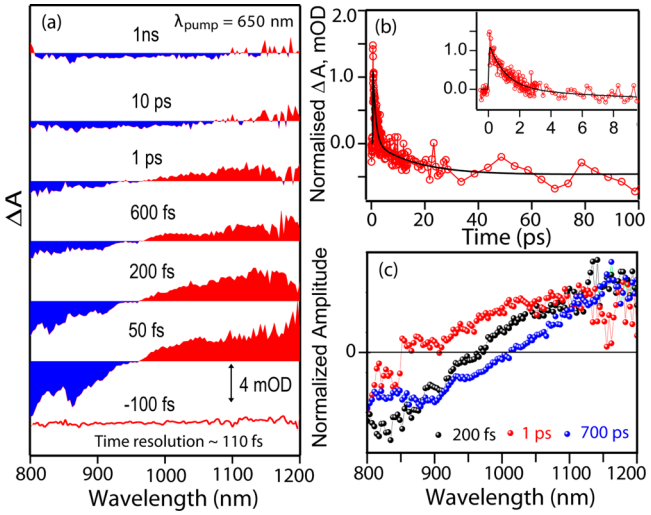

Figure 7. Transient absorption measurements of TDPP-BBT-TiO_2 film with λ_{ex} = 650 nm: (a) Different time traces representing excited state absorption at different time after excitation with resonant pump pulse. (b) Kinetic trace obtained after averaging 970−985 nm data (black) clearly demonstrates a fast decay component of ∼1 ps. After this fast decay of polaronic state emission is visible. (c) Principal spectra obtained after singular value decomposition (SVD) of pump−probe data in the NIR region. Lifetimes obtained are shown inside the plot. Time resolution of the experiment was ∼110 fs which was determined using optical kerr experiment.

represents spectral traces of polymer at different time intervals after subjecting to photoexcitation. Spectral trace at 50 fs shows a prominent negative ΔA feature of stimulated emission (in blue) spanning between 800 and 950 nm, and positive feature (in red) from 950 to 1200 nm representing polymer excited state absorption on the TiO_2 surface. Stimulated emission feature red shifts to 1050 nm within 1 ps which possibly indicates polymer relaxation on the TiO_2 surface. Kinetic trace at 1093 nm shows a time component of 0.3 ± 0.1 ps for this ultrafast relaxation process along with a long time component of 700 ps (Supporting Information, Figure S13). Similarly, kinetic trace of ESA obtained after averaging the data from 1160 to 1170 nm shows a time constant 0.2 ± 0.1 ps along with a longer time constant. However, the absorption feature at 1020 nm which appears immediately after photoexcitation decays and results in the appearance of stimulated emission signature at later times especially seen in the 10 ps trace. Kinetic trace of ESA in this region obtained after averaging 970−985 nm has been shown in Figure 7b which shows a time component of 1.2 ± 0.3 ps. It should be noted that this component is masked by the ultrafast relaxation component at red wavelengths especially >1100 nm.

To ascertain these time constants, SVD analysis was done to obtain three principal components with lifetimes of 200 fs and 1 and 700 ps (see Figure S14 in the Supporting Information) whose normalized amplitudes are shown in Figure 7c. A large amplitude 200 fs component shows a stimulated emission band at 825 nm and a broad absorption at 1150 nm which has been assigned as the singlet exciton feature of polymer on the TiO_2 surface. The 700 ps component shows red-shifted stimulated emission feature at 875 nm, representing possibly a relaxed long-lived singlet exciton state. However, a small amplitude 1 ps component shows a negative feature until 850 nm representing ground state bleach (GSB) and a broad absorption until 1200 nm. These three principal components can be sequenced in either a homogeneous scheme or an inhomogeneous kinetic model. The pronounced ground state bleach feature at <820 nm in the 1 ps component implies it represents a state which does not show any emission and possibly represents the immediately generated polaronic state. To convincingly assign this component to the hole trapped state, the component spectrum was overlaid with the ground state absorption spectrum of the polymer radical cation which was chemically generated using $FeCl_3$ in chloroform. The overlay of the radical cation and the 1 ps spectrum in Figure 8 provides a direct

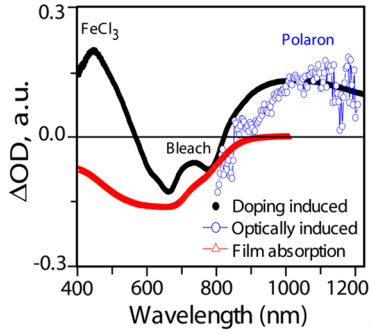

Figure 8. Comparison of polaron absorption band obtained after chemical oxidation via $FeCl_3$ (black) with the photogenerated polaron feature (blue) after exciting the TDPP-BBT−TiO_2 Film with resonant 650 nm laser pulse. Absorption spectrum of the polymer−TiO_2 film (in red) obtained through diffuse reflectance has been shown with negative amplitude to compare it directly with the transient bleach signal.

comparison of the similarity between the chemically doped polaron feature with the photogenerated state. In order to critically evaluate the crossover region to the bleach, we compared it to the diffuse reflectance spectrum obtained from the polymer−TiO_2 film (also shown in the Supporting Information, Figure S18). Figure 8 evidently shows an excellent overlap of the bleach region confirming our assignment for the 1 ps component as a photogenerated polaron state of the TDPP-BBT polymer. We do not see any evidence for the formation of a triplet state in polymer on TiO_2 which points toward a singlet injection mechanism.

The evolution of the stimulated emission and a red-shifted ESA feature as seen in the transient data is indicative of sequential connection between the 200 fs and 700 ps spectral components in the kinetic scheme. The distinct polaron state thus should arise from an independent pathway which may

dx.doi.org/10.1021/jp510733k | J. Phys. Chem. C 2014, 118, 29650−29662

have bifurcated from the initially prepared delocalized singlet exciton in a homogeneous scheme. However, the IRF limited generation and simultaneously a small yield of the polaron state implies a population fractionation which is inconsistent with a homogeneous kinetic model with excited state branching. In this context, we argue for an inhomogeneous kinetic scheme which invokes pronounced ground state heterogeneity[53] such that only a certain fraction of polymers can actually inject. The 700 ps component appears to be the major population due to large amplitude contribution, and has an emissive singlet state unlike in solution. We conjecture that the emissive population arises from creation of nonspecific polymer−TiO_2 nanocomposites or aggregates similar to the MEH-PPV-TiO_2 lasing composites previously reported by Alan Heegar and coworkers.[54,55] Imaging the polymer−TiO_2 film using scanning electron microscopy (SEM) provides support to an inhomogeneous distribution of polymer around the TiO_2 surface (Supporting Information, Figure S15).

Resonance Raman Measurements on Films. In order to critically understand the molecular nature of the ground state heterogeneity in polymer−TiO_2 interactions, we performed structure-sensitive vibrational Raman spectroscopy to characterize the bound population. Resonance Raman (RR) spectra obtained with 532 nm excitation of the free polymer in solution (black), free polymer film (red), and polymer−TiO_2 film (blue) are shown in Figure 9. The RR spectrum of free TDPP-BBT in

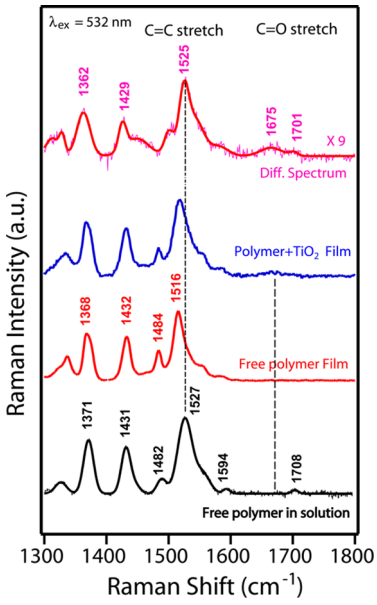

Figure 9. Normalized resonance Raman spectra of polymer free in solution (black), in film (red) and on TiO_2 film (blue) at excitation wavelength of 532 nm. Resonance Raman spectrum of TiO_2-bound polymer on film is obtained by plotting a normalized difference spectrum (pink). This spectrum has been amplified by 9 times for comparison. Polymer−TiO_2 film data clearly represents the heterogeneity in the polymer population on TiO_2 surface.

solution shows prominent peaks at 1371, 1431, and 1527 cm^{-1} corresponding to delocalized C−C/C−N and C−S stretches. There are features with low Raman cross-section at 1594 cm^{-1} which arises from the C═C stretch, and 1708 cm^{-1} emanating from localized C═O stretches from the lactam rings. The RR spectrum of polymer film shows peaks at 1368, 1432, 1484, and 1516 cm^{-1} and represents the corresponding positions of the above-described vibrational modes. The significant red-shift in the C═C stretch at 1516 cm^{-1} compared to 1527 cm^{-1} in solution along with reduction in the inhomogeneous line width of the Raman transitions imply extended conjugation lengths in the film possibly due to homogeneous ordering on the surface.

The RR spectra recorded for the polymer−TiO_2 film mirrored the free polymer spectrum although with much broader line-widths. To clearly enunciate the vibrational frequency changes associated with TiO_2 binding, a normalized difference spectrum was used to reveal the Raman spectrum of the bound fraction of polymer exclusively. The difference spectrum in pink plotted in Figure 9 has intensities almost 9 times smaller than the free polymer intensities indicative of a minor polymer fraction that is bound. The spectrum shows prominent features at 1362, 1429, 1525, 1675, and 1701 cm^{-1} corresponding to the TiO_2 bound polymer only although the 1701 cm^{-1} refers to unbound C═O groups on the DPP unit. The C═C stretch at 1525 cm^{-1} is similar to the solution which is at 1527 cm^{-1}, signifies reduced conjugation in the polymer backbone due to binding with the TiO_2 nanoparticles. It should be noted here that TiO_2 particles do not show any Raman feature in between 1000 and 1800 cm^{-1}, and the C═O stretch feature is only present in polymer−TiO_2 Raman spectrum (see Figure S16 in the Supporting Information). The remarkable decrease in the lactam ring's C═O stretching frequency from 1708 cm^{-1} in free polymer to 1675 cm^{-1} in bound form of the polymer signifies substantial lowering of the carbonyl bond-order upon binding to TiO_2.[56] The substantial red-shift of the C═O stretch can be directly correlated to the binding of this polymer to the TiO_2 surface. The peak width indicates heterogeneity in the binding process which in turn refers to weaker adsorption with large degrees of freedom on the surface and no control on the polymer adsorption angle.[57] The weak binding affinity possibly arises from the poor sigma-donating ability of the C═O group which immediately explains the experimentally obtained low bound polymer coverage over the TiO_2 surface. Therefore, the small fraction of C═O bound polymers possibly corresponds to the kinetically observed minor injecting population in the transient absorption data. Major fraction of the polymer population exhibits a long-lived singlet exciton state which arises possibly due to some specific polymeric structures formed due to nonspecific polymer−TiO_2 interactions. However, we are not ruling out the possibility of electron injection from some of the polymer molecules in the periphery of the aggregates interacting with the TiO_2.

Evaluation of ET Parameters. The electron injection time scale of <110 fs is comparable to the injection rates reported for homopolymers like polythiophenes[58] as well as small organic molecules to TiO_2.[59] This ultrafast electron injection suggests strong electronic coupling between the TDPP-BBT S_1 excited state and the TiO_2. The electronic coupling matrix element, H_{AB}, can be estimated from semiclassical Marcus theory for electron transfer:

$$k_{et} = \frac{2\pi}{\hbar}|H_{AB}|^2 \frac{1}{\sqrt{4\pi\lambda k_b T}} \exp\left[\frac{-(\Delta G^\circ + \lambda)^2}{4\lambda k_b T}\right]$$

where k_{et} = rate constant for electron transfer reaction, λ is the reorganization energy, and ΔG° is the free energy change for the reaction which is the driving force for the electron transfer. Driving force for the excited state electron transfer reaction can be calculated using Rehm−Weller equation:[60]

dx.doi.org/10.1021/jp510733k | J. Phys. Chem. C 2014, 118, 29650−29662

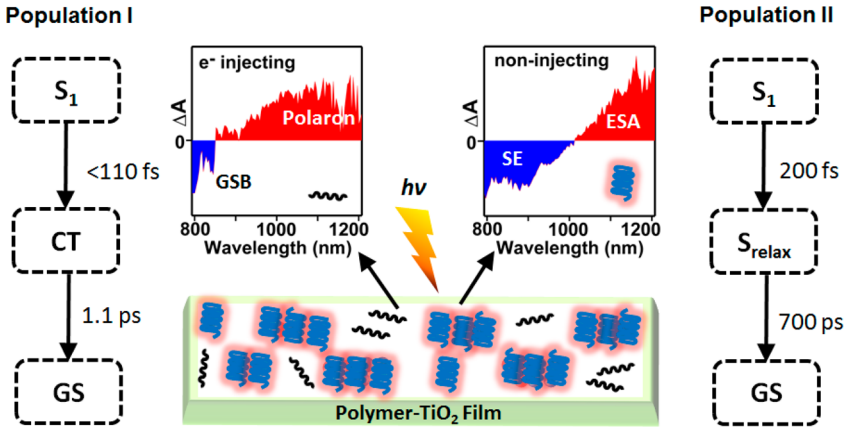

Figure 10. Kinetic scheme for photoinduced processes in TDPP-BBT−TiO_2 film: CT reaction vs polymer relaxation process. For polymer molecules bound to TiO_2 through coordinate bond (population I), CT state is generated in <110 fs which goes back to the ground state through fast charge recombination of ∼1.1 ps. For polymer−TiO_2 nanocomposites on surface (Population II), photoexcitation of the TDPP-BBT polymer populates singlet exciton, S_1 state. Initially populated S_1 state relaxes through polymer coordinates to S_{relax} state which decays to ground state in the time scale of 700 ps.

$$\Delta G^\circ = E^\circ(\text{ox}) - E^\circ(\text{red}) - E_{0-0}$$

ΔG° for the electron injection for TDPP-BBT−TiO_2 was calculated to be −0.57 eV. Under the assumption of $(\Delta G^\circ + \lambda) \approx 0$, minimal value of the H_{AB} is calculated to be ∼20 meV. This value of H_{AB} is comparable to the coupling constant of ∼17 meV reported for electron transfer from PCPDTBT polymer to CdSe quantum dots by Bradforth and co-workers.[61] For highly exergonic charge recombination process, $\lambda \ll \Delta G^\circ$ and thus, $k_{bET,}$ back electron transfer rate constant is mostly dictated by the ΔG°.[62] For back electron transfer, ΔG° is $E_C - E_{S/S+}$ where E_C is the potential of the conduction band edge (= −4.26 eV) and $E_{S/S+}$ is the ground state redox potential of the polymer. Using $E_{S/S+}$ value of −3.69 eV, ΔG° was calculated to be −0.89 eV which is smaller as compared to small organic molecule−TiO_2 back ET driving force[63] due to higher lying HOMO level in this low bandgap polymer. But contrary to the small organic molecule−TiO_2, back ET rate, 0.9×10^{12} s^{-1} is much faster in polymer. This anomaly can be explained by the rapid geminate recombination due to the small physical separation of the photoinduced charges. The delocalized HOMO on the D-A backbone leads to hole localization on DPP unit close to the TiO_2 surface. Similar ultrafast back ET from low-band gap polymers to CdSe has also been observed by Bradforth et al.[61] Therefore, the fast charge recombination process seems to be consistent with the moderate power conversion efficiency observed with TDPP-BBT polymer sensitized solar cell.[32]

Physical Model on TDPP-BBT−TiO_2 Interactions. A depictive physical model shown in Figure 10 summarizes the major conclusions from our analysis of the transient optical data along with the resonance Raman measurements on polymer−TiO_2 films. The ground state heterogeneity is depicted by showing the transient spectral signatures of two distinct polymer populations on the TiO_2 film shown in white color. The specific polymer−TiO_2 interaction through the C═O group in the DPP moiety helps in forming a chemically competent dye population shown in black. The major population however arises from a nonspecifically associated polymer population shown as emissive aggregates (in blue color) over the TiO_2 film. The aggregate population forms the noninjecting fraction which lives for ∼700 ps and is emissive. Our analysis thus indicates that it becomes imperative to gather molecular-level insight into the competitive pathways of ultrafast charge generation along with ground state heterogeneity for optimizing the TDPP-BBT, a low-band gap polymer sensitized solar cells. Therefore, characterizing these films with optical super-resolution imaging techniques which have an intrinsic molecular contrast is indeed required. New surface spectroscopic tools are emerging that will be capable of providing detailed insight into the molecular nature of these composites.[64,65]

The ultrafast time scale of electron injection into TiO_2 through the C═O group also drives the fast recombination time scale due to very favorable driving force and possibly small spatial separation between the photogenerated electron−hole pair. With a deep HOMO level one would ensure large driving force which could prevent fast back electron transfer due to the Marcus inverted region. Alternatively, we envision that tuning the electronic coupling between the donor and the DPP moiety will enhance spatial separation of the polymer localized hole and TiO_2 trapped electron, and therefore prolong the recombination lifetime. The TDPP-BBT polymer has a very TDPP centric electronic state though with small amount of electron localization on the donor unit. Once the hole is trapped on this D−A backbone, TDPP possibly retains greater fraction of the hole density which localizes the hole close to the TiO_2 surface. In order to move the charge away from the surface, it will be important to vary the linker length between the donor and the TDPP unit for facilitating the hole transfer process. The variation of the length has to be carefully optimized in conjunction with keeping the rigidity of the conformation intact to establish long conjugation lengths.[48] Additionally the specific polymer−TiO_2 interaction can be increased by side-chain engineering[66,67] on DPP unit to minimize the polymer−polymer interaction which would enhance the photovoltaic efficiency.

4. CONCLUSIONS

In conclusion, we provide the first spectroscopic analysis of charge transfer reactivity for potentially a promising group of low bandgap polymers based on diketopyrrolopyrrole molecular unit on TiO_2 surface. Direct evidence for impaired charge transfer efficiency in polymer−TiO_2 films due to fast charge

dx.doi.org/10.1021/jp510733k | J. Phys. Chem. C 2014, 118, 29650−29662

recombination rate combined with pronounced ground state heterogeneity in polymer−TiO_2 films is deduced from our steady state vibrational and transient optical spectroscopies. Although the <110 fs time scale of electron injection from polymer singlet state into TiO_2 is similar to small molecule dyes,[59,68] the back ET time-constant of ∼1.1 ps is one of the causes for the low performance of the TDPP-BBT based DSSC's. Major fraction of the polymer forms composites with TiO_2 which have surprisingly long-lived excited states that emit in the NIR region, and create nonelectron injecting population on the TiO_2 surface. These results should motivate future work to actively probe the nature of polymer−TiO_2 interactions and look for solution processes that impart greater control on film homogeneity. Molecular engineering to restrict such nonproductive populations will pave the way toward more efficient utilization of the incident photon energy. Our work also highlights the importance of gathering bond-specific information on the hole localization in such polymeric systems[69] and will provoke specific chemical modifications that will assist in preventing geminate recombination.[70]

■ ASSOCIATED CONTENT

Supporting Information

Details of the chemicals used, TCSPC measurements, steady state absorption and emission measurements on TDPP unit in solution, kinetic fitting parameters, frontier orbitals, additional time-resolved data, SEM image, and table of time-constants. This material is available free of charge via the Internet at http://pubs.acs.org.

■ AUTHOR INFORMATION

Corresponding Author

*Phone: +91-22-22782383. Fax: +91-22-22804610. E-mail: dasgupta@tifr.res.in.

Notes

The authors declare no competing financial interest.

■ ACKNOWLEDGMENTS

Authors thank Dr. Anindya Datta and his students Anjali Dhir & Avinash Kumar Singh (IIT Bombay) for upconversion measurements. Authors acknowledge Dr. G. Krishnamoorthy and Madhuri Kombrail (TIFR) for help with TCSPC measurements. Authors thank Vinayak Rane for help during the EPR measurements in TIFR. Authors also acknowledge Mr. Palas Roy, Viola D'mello, and K. Vijayalakshmi for helpful discussions. H.V.M. and V.B.Y. acknowledge the national photonics fellowship (NPF) from the Department of Information Technology, India. Dr. Jyotishman Dasgupta acknowledges department of atomic energy (DAE), India and TIFR for start-up research grant.

■ ABBREVIATIONS

DPP, diketopyrrolopyrrole; ET, electron transfer; IRF, instrument response function; ESA, excited state absorption; GSR, ground state recovery; SVD, singular value decomposition; TCSPC, time correlated single photon counting; RR, resonance Raman

■ REFERENCES

(1) Hains, A. W.; Liang, Z. Q.; Woodhouse, M. A.; Gregg, B. A. Molecular Semiconductors in Organic Photovoltaic Cells. *Chem. Rev.* **2010**, *110*, 6689−6735.
(2) Hagfeldt, A.; Boschloo, G.; Sun, L. C.; Kloo, L.; Pettersson, H. Dye-Sensitized Solar Cells. *Chem. Rev.* **2010**, *110*, 6595−6663.
(3) Hagfeldt, A.; Gratzel, M. Molecular Photovoltaics. *Acc. Chem. Res.* **2000**, *33*, 269−277.
(4) Gratzel, M. Dye-sensitized Solar Cells. *J. Photochem. Photobiol. C - Photochem. Rev.* **2003**, *4*, 145−153.
(5) Nozik, A. J.; Miller, J. Introduction to Solar Photon Conversion. *Chem. Rev.* **2010**, *110*, 6443−6445.
(6) Kim, J. Y.; Lee, K.-S.; Coates, N. E.; Moses, D.; Nguyen, T.-Q.; Dante, M.; Heeger, A. J. Efficient Tandem Polymer Solar Cells Fabricated by All-Solution Processing. *Science* **2007**, *317*, 222−225.
(7) Li, C.; Liu, M.; Pschirer, N. G.; Baumgarten, M.; Müllen, K. Polyphenylene-based Materials for Organic Photovoltaics. *Chem. Rev.* **2010**, *110*, 6817−6855.
(8) Günes, S.; Neugebauer, H.; Sariciftci, N. S. Conjugated Polymer-based Organic Solar Cells. *Chem. Rev.* **2007**, *107*, 1324−1338.
(9) Nayak, P. K.; Bisquert, J.; Cahen, D. Assessing Possibilities and Limits for Solar Cells. *Adv. Mater.* **2011**, *23*, 2870−2876.
(10) Shevaleevskiy, O. The Future of Solar Photovoltaics: A New Challenge for Chemical Physics. *Pure Appl. Chem.* **2008**, *80*, 2079−2089.
(11) Clarke, T. M.; Durrant, J. R. Charge Photogeneration in Organic Solar Cells. *Chem. Rev.* **2010**, *110*, 6736−6767.
(12) Oregan, B.; Gratzel, M. A Low-cost High-efficiency Solar-cell based on Dye-sensitized collidal TiO_2 Films. *Nature* **1991**, *353*, 737−740.
(13) Yum, J. H.; Holcombe, T. W.; Kim, Y.; Yoon, J.; Rakstys, K.; Nazeeruddin, M. K.; Gratzel, M. Towards High-performance DPP-based Sensitizers for DSC Applications. *Chem. Commun.* **2010**, *48*, 10727−10729.
(14) Jørgensen, M.; Norrman, K.; Krebs, F. C. Stability/degradation of Polymer Solar Cells. *Sol. Energy Mater. Sol. Cells* **2008**, *92*, 686−714.
(15) Mishra, A.; Fischer, M. K. R.; Bauerle, P. Metal-Free Organic Dyes for Dye-Sensitized Solar Cells: From Structure: Property Relationships to Design Rules. *Angew. Chem. Int. Ed.* **2009**, *48*, 2474−2499.
(16) Mathew, S.; Yella, A.; Gao, P.; Humphry-Baker, R.; Curchod, B. F. E.; Ashari-Astani, N.; Tavernelli, I.; Rothlisberger, U.; Nazeeruddin, M. K.; Graetzel, M. Dye-sensitized Solar Cells with 13% Efficiency Achieved through the Molecular Engineering of Porphyrin Sensitizers. *Nat. Chem.* **2013**, *6*, 242−247.
(17) Cheng, Y. J.; Yang, S. H.; Hsu, C. S. Synthesis of Conjugated Polymers for Solar Cell Applications. *Chem. Rev.* **2009**, *109*, 5868−5923.
(18) Gendron, D.; Leclerc, M. New Conjugated Polymers for Organic Solar Cells. *Energy Environ. Sci.* **2011**, *4*, 1225−1237.
(19) Nogueira, A. F.; Longo, C.; De Paoli, M. A. Polymers in Dye Sensitized Solar Cells: Overview and Perspectives. *Coord. Chem. Rev.* **2004**, *248*, 1455−1468.
(20) Heeger, A. J. Semiconducting Polymers: the Third Generation. *Chem. Soc. Rev.* **2010**, *39*, 2354−2371.
(21) McNeill, C. R.; Greenham, N. C. Conjugated-Polymer Blends for Optoelectronics. *Adv. Mater.* **2009**, *21*, 3840−3850.
(22) Chandran, D.; Lee, K.-S. Diketopyrrolopyrrole: A Versatile Building Block for Organic Photovoltaic Materials. *Macromol. Res.* **2013**, *21*, 272−283.
(23) Li, Y.; Sonar, P.; Murphy, L.; Hong, W. High Mobility Diketopyrrolopyrrole (DPP)-based Organic Semiconductor Materials for Organic Thin Film Transisters and Photovoltaics. *Energy Environ. Sci.* **2013**, *6*, 1684−1710.
(24) Qu, S. Y.; Wang, B.; Guo, F. L.; Li, J.; Wu, W. J.; Kong, C.; Long, Y. T.; Hua, J. L. New Diketo-pyrrolo-pyrrole (DPP) Sensitizer Containing a Furan Moiety for Efficient and Stable Dye-sensitized Solar Cells. *Dyes Pigm.* **2012**, *92*, 1384−1393.
(25) Kanimozhi, C.; Yaacobi-Gross, N.; Chou, K. W.; Amassian, A.; Anthopoulos, T. D.; Patil, S. Diketopyrrolopyrrole-Diketopyrrolopyrrole-Based Conjugated Copolymer for High-Mobility Organic Field-Effect Transistors. *J. Am. Chem. Soc.* **2012**, *134*, 16532−16535.

(26) Ripaud, E.; Demeter, D.; Rousseau, T.; Boucard-Cetol, E.; Allain, M.; Po, R.; Leriche, P.; Roncali, J. Structure-properties Relationships in Conjugated Molecules Based on Diketopyrrolopyrrole for Organic Photovoltaics. *Dyes Pigm.* **2012**, *95*, 126−133.
(27) Bronstein, H.; Chen, Z.; Ashraf, R. S.; Zhang, W.; Du, J.; Durrant, J. R.; Shakya Tuladhar, P.; Song, K.; Watkins, S. E.; Geerts, Y.; et al. Thieno[3,2-b]thiophene-diketopyrrolopyrrole-containing Polymers for High-performance Organic Field-effect Transistors and Organic Photovoltaic Devices. *J. Am. Chem. Soc.* **2011**, *133*, 3272−3275.
(28) Hao, Z.; Iqbal, A. Some Aspects of Organic Pigments. *Chem. Soc. Rev.* **1997**, *26*, 203−213.
(29) Zhang, F.; Jiang, K. J.; Huang, J. H.; Yu, C. C.; Li, S. G.; Chen, M. G.; Yang, L. M.; Song, Y. L. A Novel Compact DPP Dye with Enhanced Light Harvesting and Charge Transfer Properties for Highly Efficient DSCs. *J. Mater. Chem. A* **2013**, *1*, 4858−4863.
(30) Holcombe, T. W.; Yum, J. H.; Yoon, J.; Gao, P.; Marszalek, M.; Di Censo, D.; Rakstys, K.; Nazeeruddin, M. K.; Graetzel, M. A Structural Study of DPP-based Sensitizers for DSC Applications. *Chem. Commun.* **2012**, *48*, 10724−10726.
(31) Zoombelt, A. P.; Mathijssen, S. G. J.; Turbiez, M. G. R.; Wienk, M. M.; Janssen, R. A. J. Small Band Gap Polymers Based on Diketopyrrolopyrrole. *J. Mater. Chem.* **2010**, *20*, 2240−2246.
(32) Kanimozhi, C.; Balraju, P.; Sharma, G. D.; Patil, S. Diketopyrrolopyrrole-Based Donor-Acceptor Copolymers as Organic Sensitizers for Dye Sensitized Solar Cells. *J. Phys. Chem. C* **2010**, *114*, 3287−3291.
(33) Moghe, D.; Yu, P.; Kanimozhi, C.; Patil, S.; Guha, S. Charge Transfer Complex States in Diketopyrrolopyrrole Polymers and Fullerene Blends: Implications for Organic Solar Cell Efficiency. *Appl. Phys. Lett.* **2011**, *99*, 233307.
(34) Bredas, J. L.; Norton, J. E.; Cornil, J.; Coropceanu, V. Molecular Understanding of Organic Solar Cells: The Challenges. *Acc. Chem. Res.* **2009**, *42*, 1691−1699.
(35) Hoffman, D. P.; Lee, O. P.; Millstone, J. E.; Chen, M. S.; Su, T. A.; Creelman, M.; Frechet, J. M. J.; Mathies, R. A. Electron Transfer Dynamics of Triphenylamine Dyes Bound to TiO2 Nanoparticles from Femtosecond Stimulated Raman Spectroscopy. *J. Phys. Chem. C* **2013**, *117*, 6990−6997.
(36) Rajh, T.; Chen, L. X.; Lukas, K.; Liu, T.; Thurnauer, M. C.; Tiede, D. M. Surface Restructuring of Nanoparticles: An Efficient Route for Ligand-metal Oxide Crosstalk. *J. Phys. Chem. B* **2002**, *106*, 10543−10552.
(37) Banerji, N.; Cowan, S.; Leclerc, M.; Vauthey, E.; Heeger, A. J. Exciton Formation, Relaxation, and Decay in PCDTBT. *J. Am. Chem. Soc.* **2010**, *132*, 17459−17470.
(38) Jha, A.; Chakraborty, D.; Srinivasan, V.; Dasgupta, J. Photoinduced Charge Transfer in Solvated Anthraquinones Is Facilitated by Low-Frequency Ring Deformations. *J. Phys. Chem. B* **2013**, *117*, 12276−12285.
(39) Chatterjee, S.; Burai, T. N.; Karuso, P.; Datta, A. Ultrafast Dynamics of Epicocconone, a Second Generation Fluorescent Protein Stain. *J. Phys. Chem. A* **2011**, *115*, 10154−10158.
(40) Kanimozhi, C.; Balraju, P.; Sharma, G. D.; Patil, S. Synthesis of Diketopyrrolopyrrole Containing Copolymers: A Study of Their Optical and Photovoltaic Properties. *J. Phys. Chem. B* **2010**, *114*, 3095−3103.
(41) Hwang, I.; Scholes, G. D. Electronic Energy Transfer and Quantum-Coherence in π-Conjugated Polymers. *Chem. Mater.* **2011**, *23*, 610−620.
(42) Martin, T. P.; Wise, A. J.; Busby, E.; Gao, J.; Roehling, J. D.; Ford, M. J.; Larsen, D. S.; Moulé, A. J.; Grey, J. K. Packing Dependent Electronic Coupling in Single Poly(3-hexylthiophene) H- and J-Aggregate Nanofibers. *J. Phys. Chem. B* **2013**, *117*, 4478−4487.
(43) van Hal, P. A.; Christiaans, M. P. T.; Wienk, M. M.; Kroon, J. M.; Janssen, R. A. J. Photoinduced Electron Transfer from Conjugated Polymers to TiO2. *J. Phys. Chem. B* **1999**, *103*, 4352−4359.
(44) Coronado, J. M.; Maira, A. J.; Conesa, J. C.; Yeung, K. L.; Augugliaro, V.; Soria, J. EPR Study of the Surface Characteristics of Nanostructured TiO2 under UV Irradiation. *Langmuir* **2001**, *17*, 5368−5374.
(45) Gieseking, B.; Jack, B.; Preis, E.; Jung, S.; Forster, M.; Scherf, U.; Deibel, C.; Dyakonov, V. Excitation Dynamics in Low Band Gap Donor-Acceptor Copolymers and Blends. *Adv. Energy Mater.* **2012**, *2*, 1477−1482.
(46) Banerji, N.; Cowan, S.; Vauthey, E.; Heeger, A. J. Ultrafast Relaxation of the Poly(3-hexylthiophene) Emission Spectrum. *J. Phys. Chem. C* **2011**, *115*, 9726−9739.
(47) Malinowski, E. R. *Factor Analysis in Chemistry*, 2nd ed.; John Wiley and Sons: New York, 1991.
(48) Jackson, N. E.; Savoie, B. M.; Kohlstedt, K. L.; Olvera de la Cruz, M.; Schatz, G. C.; Chen, L. X.; Ratner, M. A. Controlling Conformations of Conjugated Polymers and Small Molecules: The Role of Nonbonding Interactions. *J. Am. Chem. Soc.* **2013**, *135*, 10475−10483.
(49) Busby, E.; Carroll, E. C.; Chinn, E. M.; Chang, L. L.; Moule, A. J.; Larsen, D. S. Excited-State Self-Trapping and Ground-State Relaxation Dynamics in Poly(3-hexylthiophene) Resolved with Broadband Pump-Dump-Probe Spectroscopy. *J. Phys. Chem. Lett.* **2011**, *2*, 2764−2769.
(50) Yu, W.; Zhou, J.; Bragg, A. E. Exciton Conformational Dynamics of Poly(3-hexylthiophene) (P3HT) in Solution from Time-Resolved Resonant-Raman Spectroscopy. *J. Phys. Chem. Lett.* **2012**, *3*, 1321−1328.
(51) Karsten, B. P.; Bouwer, R. K. M.; Hummelen, J. C.; Williams, R. M.; Janssen, R. A. J. Charge Separation and (Triplet) Recombination in Diketopyrrolopyrrole-fullerene Triads. *Photochem. Photobiol. Sci.* **2010**, *9*, 1055−1065.
(52) Jailaubekov, A. E.; Vengris, M.; Song, S.-H.; Kusumoto, T.; Hashimoto, H.; Larsen, D. S. Deconstructing the Excited-State Dynamics of beta-Carotene in Solution. *J. Phys. Chem. A* **2011**, *115*, 3905−3916.
(53) Kim, P. W.; Rockwell, N. C.; Martin, S. S.; Lagarias, J. C.; Larsen, D. S. Heterogeneous Photodynamics of the P-fr State in the Cyanobacteriai Phytochrome Cph1. *Biochemistry* **2014**, *53*, 4601−4611.
(54) Hide, F.; Schwartz, B. J.; DiazGarcia, M. A.; Heeger, A. J. Laser Emission from Solutions and Films containing Semiconducting Polymer and Titanium Dioxide Nanocrystals. *Chem. Phys. Lett.* **1996**, *256*, 424−430.
(55) Carter, S. A.; Scott, J. C.; Brock, P. J. Enhanced Luminance in Polymer Composite Light Emitting Devices. *Appl. Phys. Lett.* **1997**, *71*, 1145−1147.
(56) Shoute, L. C.; Loppnow, G. R. Excited-state Metal-to-ligand Charge Transfer Dynamics of a Ru(II) Dye in Solution Adsorbed on TiO_2 Nanoparticles from Resonance Raman Spectroscopy. *J. Am. Chem. Soc.* **2003**, *125*, 15636−15646.
(57) Huber, R.; Moser, J. E.; Gratzel, M.; Wachtveitl, J. Real-time Observation of Photoinduced Adiabatic Electron Transfer in Strongly Coupled Dye/Semiconductor Colloidal Systems with a 6 fs Time Constant. *J. Phys. Chem. B* **2002**, *106*, 6494−6499.
(58) Ai, X.; Anderson, N.; Guo, J.; Kowalik, J.; Tolbert, L. M.; Lian, T. Ultrafast Photoinduced Charge Separation Dynamics in Polythiophene/SnO_2 Nanocomposites. *J. Phys. Chem. B* **2006**, *110*, 25496−25503.
(59) Watson, D. F.; Meyer, G. J. Electron Injection at Dye-sensitized Semiconductor Electrodes. *Annu. Rev. Phys. Chem.* **2005**, *56*, 119.
(60) Rehm, D.; Weller, A. Kinetics of Fluorescence Quenching by Electron and H-atom Transfer. *Israel J. Chem.* **1970**, *8*, 259.
(61) Couderc, E.; Greaney, M. J.; Brutchey, R. L.; Bradforth, S. E. Direct Spectroscopic Evidence of Ultrafast Electron Transfer from a Low Band Gap Polymer to CdSe Quantum Dots in Hybrid Photovoltaic Thin Films. *J. Am. Chem. Soc.* **2013**, *135*, 18418−18426.
(62) Banerjee, T.; Kaniyankandy, S.; Das, A.; Ghosh, H. N. Synthesis, Steady-State, and Femtosecond Transient Absorption Studies of Resorcinol Bound Ruthenium(II)- and Osmium(II)-polypyridyl Complexes on Nano-TiO_2 Surface in Water. *Inorg. Chem.* **2013**, *52*, 5366−5377.

(63) Banerjee, T.; Biswas, A. K.; Reddy, U. G.; Sahu, T. S.; Das, A.; Ganguly, B.; Ghosh, H. N. Superior Grafting and State-of-the-Art Interfacial Electron Transfer Rates for Newly Designed Geminal Dicarboxylate Bound Ruthenium(II)- and Osmium(II)-Polypyridyl Dyes on TiO_2 Nanosurface. *J. Phys. Chem. C* **2014**, *118*, 3864−3877.
(64) Chappell, J.; et al. Correlating Structure with Fluorescence Emission in Phase-separated Conjugated-Polymer Blends. *Nat. Mater.* **2003**, *2*, 616−621.
(65) Rajapaksa, I.; Wickramasinghe, H. K. Raman Spectroscopy and Microscopy Based on Mechanical Force Detection. *Appl. Phys. Lett.* **2011**, *99*.
(66) Mei, J.; Bao, Z. Side Chain Engineering in Solution-Processable Conjugated Polymers. *Chem. Mater.* **2014**, *26*, 604.
(67) Cui, C.; Wong, W.-Y.; Li, Y. Improvement of Open-circuit Voltage and Photovoltaic Properties of 2D-Conjugated Polymers by Alkylthio Substitution. *Energy Environ. Sci.* **2014**, *7*, 2276−2284.
(68) Anderson, N.; Lian, T. Ultrafast Electron Transfer at Molecule-Semiconductor Nanoparticle Interface. *Annu. Rev. Phys. Chem.* **2005**, *56*, 491−519.
(69) Frontiera, R. R.; Dasgupta, J.; Mathies, R. A. Probing Interfacial Electron Transfer in Coumarin 343 Sensitized TiO_2 Nanoparticles with Femtosecond Stimulated Raman. *J. Am. Chem. Soc.* **2009**, *131*, 15630.
(70) Hu, K.; Robson, K. C. D.; Beauvilliers, E. E.; Schott, E.; Zarate, X.; Arratia-Perez, R.; Berlinguette, C. P.; Meyer, G. J. Intramolecular and Lateral Intermolecular Hole Transfer at the Sensitized TiO_2 Interface. *J. Am. Chem. Soc.* **2014**, *136*, 1034−1046.